JOURNAL OF MATERIALS SCIENCE 31 (1996) 983–993

Matrix-dominated tensile behaviour of unidirectional T300/914 and structural modelling of the material

A. LOWE*
Department of Materials Science, University of Cambridge, Pembroke Street, Cambridge CB2 3QZ, UK

Unidirectional T300/914 carbon epoxy composite has been tested under transverse tensile loading at various temperatures and test rates. The test programme revealed a different viscoelastic response for the bulk resin modulus from that of the composite modulus and associated fractographic examination showed the structures of the resin and composite to be complex. The resin consisted of an epoxy-based particulate phase embedded within a thermoplastic-based connecting phase. The addition of carbon fibres resulted in the formation of an irregular epoxy-based interphase region. A parameter, Λ, has been defined that easily characterizes the viscoelastic behaviour of the composite. Structural models have been successfully developed for both the resin and the composite and a cure mechanism suggested. Any plastic deformation occurring on failure was within the connecting phase and the weakest point of the composite was identified as being the particle/interphase boundary. Property modelling has successfully accounted for the interphase influence on the transverse tensile modulus and the composite transverse tensile strength was found to be higher than the bulk resin tensile strength.

1. Introduction

Epoxy resins form one of the most important and largest materials groups in use today. Initially used as adhesives, tooling and potting compounds, epoxy resins are now also used in the aviation industry as matrix materials for fibre-reinforced composite structures. Unfortunately, epoxy resins have poor notch resistance and lose much of their structural integrity when damaged. Epoxy resin development as matrix materials began in the early 1950s [1], because their excellent adhesion characteristics, especially to carbon fibres, and the low shrinkage experienced on curing, gave them an advantage over other resin systems.

Behind every successful composites application has to lie an understanding of basic material properties upon which structural design is based. This understanding usually manifests itself in the form of unidirectional laminate properties which are then expanded by various laminate theories into well-defined design variables. Tensile properties in the longitudinal direction tend to receive the most attention, because this direction provides most of the desired structural strength and stiffness. Transverse tensile properties are not so well documented, although their consideration is vitally important when designing as they usually define the weakest points in the structure. Competent design techniques have succeeded in minimizing, but not eliminating, these weaknesses. Service conditions, such as variations in temperature and strain rate, have a much greater effect in the transverse direction, due to the viscoelastic nature of the matrix. Understanding the mechanical response of a material under such conditions is vital, especially for industries such as aerospace.

Under transverse loading, damage initiation and propagation in a unidirectional composite is caused by matrix cracking and delamination at the interface. Both these failure processes are dependent upon the nature of the resin. Therefore, the development of new resin systems and the modification of existing ones to improve both toughness and strength are very important areas of research.

Measurement of the transverse modulus is straightforward, whereas measurement of transverse strength in brittle materials, such as carbon/epoxy is complicated by an acute sensitivity due to factors such as processing. This problem is not easily overcome. Literature relating to transverse tensile properties is available [2–7], but the effect of temperature and strain rate has largely been ignored.

1.1. Types of epoxy resins

Diglycidyl ether of bisphenol A (DGEBA) epoxy resin is the most common type and forms some 95% of

Present address: Faculty of Engineering and Information Technology, Department of Engineering, The Australian National University, Canberra ACT 0200 Australia

0022–2461

all epoxy resin manufacture [8]. They range from medium viscosity liquids to high melting point solids. There are four other main types of epoxy resin in use; glycidylester resins, glycidyl amine resins, novalacs and brominated epoxy resins. Of these, only glycidyl amine resins find frequent use as a commercial resin in the field of composites. One such resin is Ciba-Geigy 914.

1.2. Modification of epoxy resins

Unmodified epoxy resins have poor toughness characteristics (typically $G_{IC} = 70\ J\ m^{-2}$) [9] and are therefore unsuitable for most composites applications. A standard solution to this problem is to add toughness-enhancing substances to the resin. There are three approaches. (A) Rubber toughening [10–13], whereby liquid rubber is dissolved and dispersed within the epoxy, and then precipitates out into spherical particles on curing. Here, the increased toughness is countered by decreases in strength, modulus and glass transition temperature. (B) Particle toughening [9, 14, 15] whereby hard particles, such as glass, alumina and zirconia, are added in small amounts to epoxy resins resulting in increases in strength, modulus and toughness. (C) Thermoplastic toughening [16, 17] whereby the toughness of an epoxy resin is improved by blending with a thermoplastic constituent, such as poly(ethersulphone) (PES). 914 is an example of an epoxy resin modified thermoplastically by the addition of small amounts of PES.

1.3. Addition of PES to epoxy resin

The homogeneous mixture produced when PES and an epoxy resin are blended will undergo phase separation on curing. Bucknall and Partridge [17] produced a thermoplastic-toughened resin by dissolving PES into ERL0510 epoxy at 150 °C, cooling to 130 °C and then adding MY720 epoxy resin, followed by assorted hardeners. A complex multistage curing process took place resulting in a two-phase material. One phase was in the form of small particles approximately 1 μm in diameter, embedded within a connecting phase. The particulate phase was reported to be PES-based and the connecting phase epoxy-based. Work by Yamanaka and Inoue [16] revealed that the size of the particles was dependent upon curing parameters and compound formulation and that it was the connecting phase that was rich in PES.

Spinodal decomposition on curing is known to be the mechanism behind the formation of this two-phase structure [16]. The mechanisms behind spinodal-phase separation are complex and primarily involve thermodynamic and kinetic factors. Curing of the resin results in an increase in molecular weight, which lowers the configurational entropy of mixing [18]. This results in the enthalpy term (usually endothermic) becoming increasingly important in determining the free energy of mixing. Also, the enthalpy of mixing is altered by the opening of the epoxy ring and the formation of polar hydroxyl groups. Calculation of solubility parameters [19] has shown that this alone will cause the PES phase to separate from solution. Reaction kinetics must also be considered [20] as the choice of resin and hardener will determine the reaction rate at any given temperature.

This paper fully characterizes the matrix-dominated tensile fracture behaviour of T300/914 – a commercially available prepreg system – over specified test-rate and temperature ranges. To understand fully the fracture mechanisms involved in this characterization, the microstructure of the resin and the composite need to be fully understood. The work presented in this paper concerns development of structural models for the composite and the bulk resin based on the experimental results obtained and their use in explaining the behaviour observed during tensile fracture of unidirectional laminates over the specified test ranges.

2. Experimental procedure

2.1. Test material

T300/914 consists of carbon fibres embedded within a blend of tetraglycidyldiaminodiphenyl methane (MY720) and triglycidylparaaminophenol (ERL0510) hardened with dicyanodiamide (DDA) and/or diaminodiphenylsulphone (DDS), to which is added a small percentage of PES [21]. PES is added to reduce the chemical sensitivity of the resin and to control flow during gelation and cure. The composite was obtained in prepreg form from Ciba-Geigy plc, Duxford, UK, and processed into unidirectional laminates of two thicknesses (16 plies and 24 plies) by Rolls Royce plc, Derby, UK [22]. Bulk resin panels were obtained from Ciba-Geigy plc, Marly, Switzerland, in sheet form, 2 mm thick and 200 mm square, and possessed a glass transition temperature of 180 °C [23].

In its cured state, T300/914 has been reported to have a complex microstructure, consisting of fibres embedded within a two-phase resin matrix and possibly surrounded by an interphase region [24].

2.2. Test programme

All tensile specimens were of standard test geometry [4, 5]. Each composite specimen was 16 plies (2.2 mm) thick, 15 mm wide, 150 mm long and tabbed at each end with glass cloth/epoxy tabs, 2 mm thick and 55 mm long with a 30° taper towards the specimen gauge length (unless otherwise stated). All tabs were bonded to the specimens using Ciba-Geigy 2007 single component adhesive. The bulk resin specimens were of reduced dimensions (10 mm wide, 90 mm long with 30 mm tabs) to account for the reduced sheet thickness and to maximize the total number of specimens available from the sheets. An Instron 8032 Servo-Hydraulic test frame fitted with an environmental chamber was used for all testing.

The tests were performed over a temperature range of -40 °C to 140 °C at 20 °C intervals at a test rate of 10^0 mm min^{-1}. The test rate range varied from 10^{-2} to 10^2 mm min^{-1} at 10^1 intervals at ambient temperature (23 °C). Modulus, strength and fracture strain data were obtained from stress/strain plots. Selected specimens were then examined using scanning electron microscopy to reveal the morphology and

structure of the fracture surfaces under several test conditions. Several polished and etched transverse surfaces were also prepared for optical examination. The tensile data were then used to produce viscoelastic property models and the microscopic results were used to formulate structural models for the bulk resin and for the composite.

3. Experimental results

3.1. Transverse tensile test results

The variation of transverse tensile strength, $\sigma_{\perp T}$, with temperature, T, is shown in Fig. 1. The relationship was linear and is described by

$$\sigma_{\perp T} = 67.65 - 7.11\left(\frac{T}{T_0} - 1\right) \quad (1)$$

where 67.65 MPa is the reference transverse tensile strength at the reference temperature, T_0 (taken throughout this study as 23 °C). The increased experimental scatter at low temperatures was attributed to increased brittleness in the material. Fig. 1 also shows the results of tests involving bulk resin tensile specimens at selected temperatures. It appeared that the strength of the resin was lower than the transverse strength of the composite. This is in agreement with tests performed at Ciba-Geigy [25] and is not so for most polymer composite systems. The variation of transverse tensile strength with log test rate, R, is shown in Fig. 2, revealing an increase in strength with increasing test rate. Equation 2 best describes the linear relationship

$$\sigma_{\perp T} = 81.23 + 5.28\left(\frac{R}{R_0} - 1\right) \quad (2)$$

where R_0 is a reference log test rate value (taken throughout this study as 1, i.e. 10^1 mm min^{-1}).

Similar relationships for the variation of transverse tensile modulus, $E_{\perp T}$, with temperature and test rate are shown in Figs 3 and 4, respectively. The property variations were identical to those for strength and are described by Equations 3 and 4, respectively

$$E_{\perp T} = 9.59 - 0.515\left(\frac{T}{T_0} - 1\right) \quad (3)$$

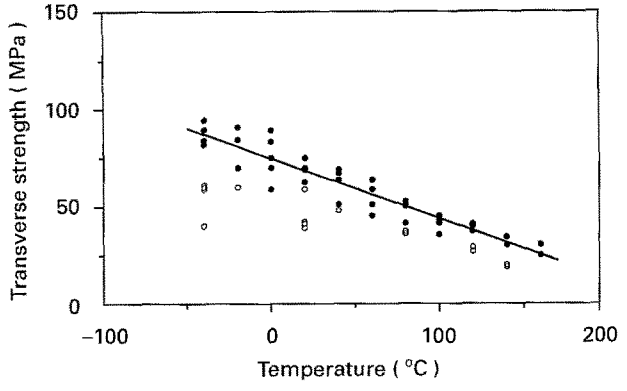

Figure 1 Variation of (●) transverse tensile strength with temperature (test rate = 1 mm min^{-1}) for unidirectional T300/914, (○) tensile bulk resin strength data.

$$E_{\perp T} = 9.86 + 0.31\left(\frac{R}{R_0} - 1\right) \quad (4)$$

The lower experimental scatter was expected, as inherent flaws have more effect on micro-properties such as strength, than on macro-properties, such as modulus. Fig. 3 also shows the variation of bulk resin tensile modulus, E_{rT}, with temperature, again obtained [25].

Figs 5 and 6 show the variation in transverse tensile fracture strain, $\varepsilon_{\perp T}$, with temperature and test-rate, respectively. The data presented represent average

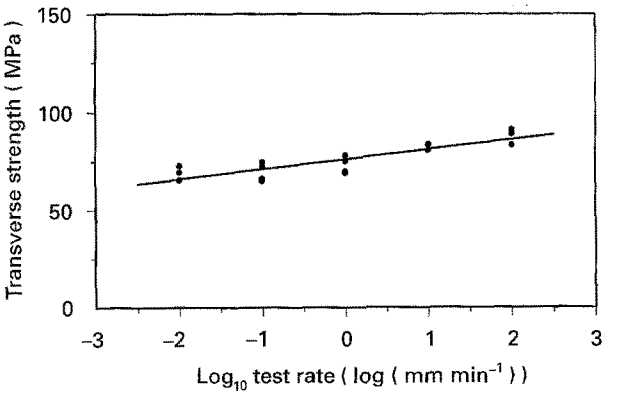

Figure 2 Variation of transverse tensile strength with test rate (temperature = 23 °C) for unidirectional T300/914.

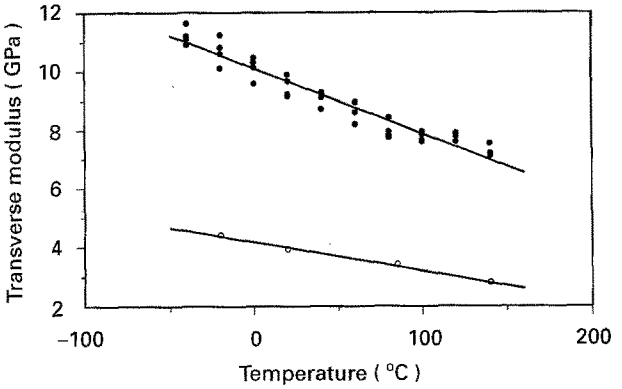

Figure 3 Variation of (●) transverse tensile modulus and (○) resin tensile modulus [25] with temperature (test rate = 10° mm min^{-1}) for unidirectional T300/914 (tensile bulk resin modulus data also included [25]).

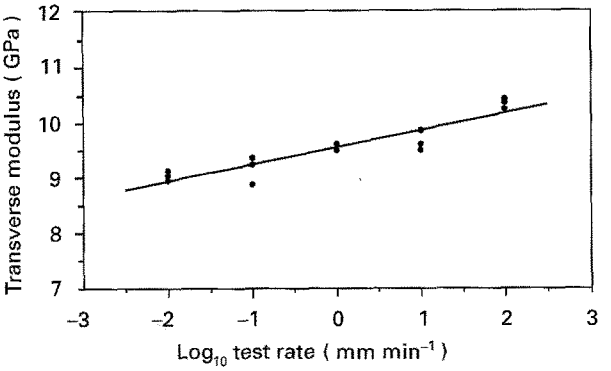

Figure 4 Variation of transverse tensile modulus with test rate (temperature = 23 °C) for unidirectional T300/914.

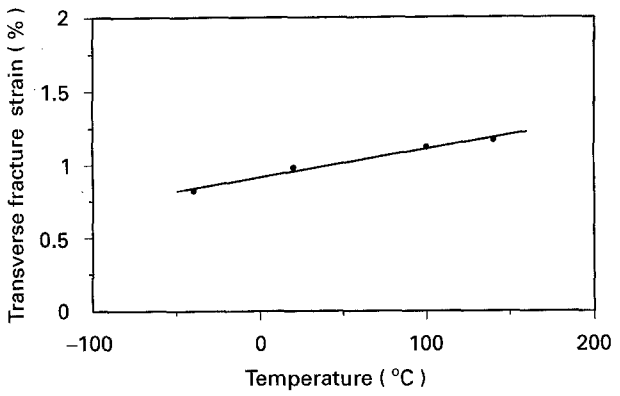

Figure 5 Variation of transverse tensile fracture strain with temperature (test rate = 1 mm min^{-1}) for unidirectional T300/914.

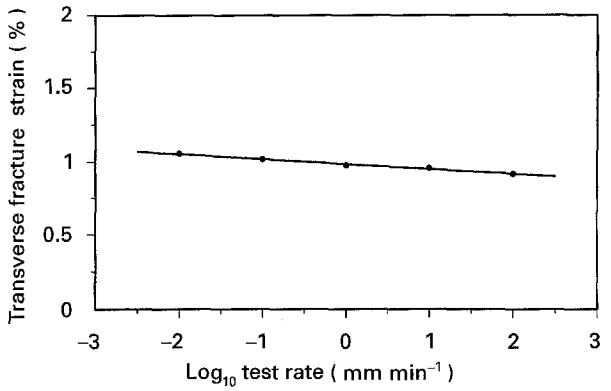

Figure 6 Variation of transverse tensile fracture strain with test rate (temperature = 23 °C) for unidirectional T300/914.

values. The strain values were low and of similar magnitude to those for the actual fibres, illustrating the brittle nature of the material. The trends observed are best described by Equations 5 and 6

$$\varepsilon_{\perp T} = 0.96 - 0.044\left(\frac{T}{T_0} - 1\right) \quad (5)$$

$$\varepsilon_{\perp T} = 0.98 - 0.034\left(\frac{R}{R_0} - 1\right) \quad (6)$$

The stress/strain response of unidirectional T300/914 tested in transverse tension at temperatures of −40, 23 and 140 °C (test rate = 10° mm min^{-1}) is shown in Fig. 7. Although the fracture strains are rather low, the levels of plastic deformation observed are substantial, especially at the higher temperatures.

3.2. Viscoelastic characterization of the material

A predetermined strength value can be obtained at a particular temperature (at a standard test rate of 10° mm min^{-1}) and also at a particular test rate (at standard temperature), illustrating the viscoelastic nature of this material under matrix-dominated loading. Temperature and test rate have much less influence on longitudinal and cross-ply properties because of the dominance of the fibres, which are relatively insensitive to the test variables. In terms of design and application, it is often useful to have this interrelation

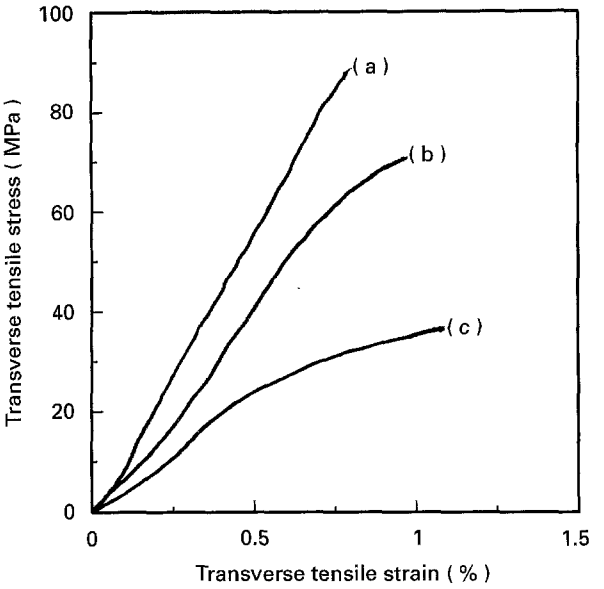

Figure 7 Stress/strain curves obtained for unidirectional T300/914 under transverse tensile loading obtained at 1 mm/min and at (a) −40 °C, (b) 23 °C and (c) 140 °C.

defined on a comparison basis, i.e. in terms of the temperature change required at a standard test rate to attain a strength variation caused by a unit test-rate variation at a standard temperature (or vice versa). This ratio (termed Λ in this study) can be defined for all properties under test. For instance, from Equation 1, $\sigma_{\perp T}$ changes with temperature at a rate of 0.309 MPa °C^{-1} (at $R = R_0$) and from Equation 2, $\sigma_{\perp T}$ changes with log test rate at a rate of 5.28 MPa min mm^{-1} (at $T = T_0$). Therefore, $\Lambda = 17.10$ min °C mm^{-1}, i.e. the transverse tensile strength of T300/914, initially under standard conditions, changes as much over a temperature range of 17.10 °C as it does over a test-rate range of 10^1 mm min^{-1}. This single parameter defines the viscoelastic response of a particular mechanical property. The values of Λ for all the properties investigated in this study are reported in Table I.

TABLE I The values of the viscoelastic parameter, Λ, for the properties of unidirectional T300/914 under study (units = °C min/mm).

Property	Λ (°C min mm^{-1})
$\sigma_{\perp T}$	17.10
$E_{\perp T}$	13.84
$\varepsilon_{\perp T}$	17.77

3.3. Fractographic examination of bulk resin and composite fracture surfaces

Fig. 8 shows a bulk resin tensile fracture surface obtained at 23 °C and at a test rate of 10° mm min^{-1}. 914 resin appears to be a two-phase structure consisting of a particulate phase, approximately 1 μm in diameter, embedded within a connecting phase. The particulate phase is the dominant structure and forms approximately 85% of the total structure. For an array of spherical particles, this is impossible, and so there

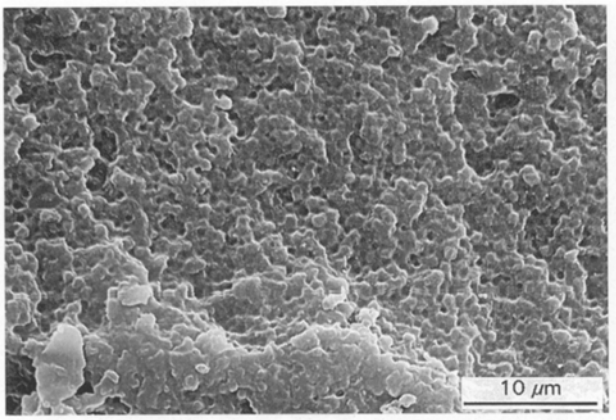

Figure 8 Tensile fracture morphology of bulk 914 resin tested at 10° mm min^{-1} and at 23 °C, revealing the two-phase nature of the structure.

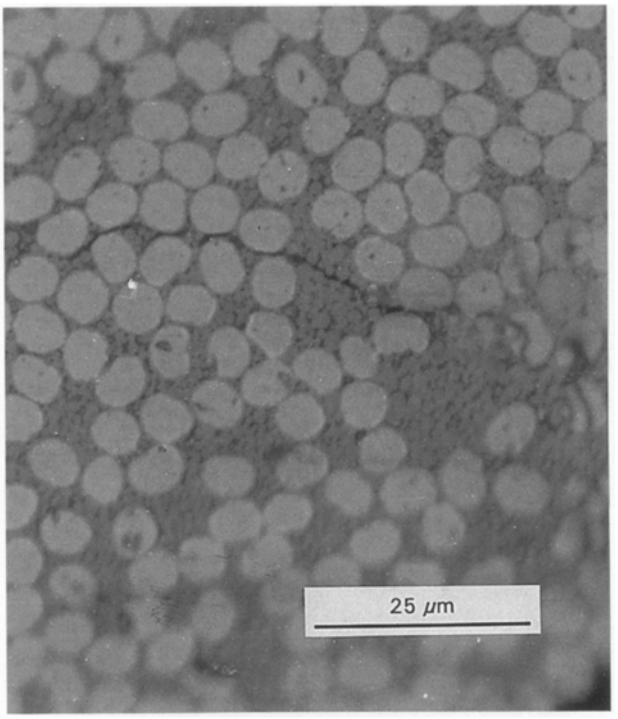

Figure 9 Polished and etched composite transverse surface with crack, showing the nature of the particulate phase, crack propagation path and the interphase region around the fibres.

must be regions where the particulate phase has fused together to form larger particles. Fig. 9 shows a polished composite specimen etched in methylene chloride. The particulate phase appears irregular in size and shape, suggesting that fused regions are present. The connecting phase has been attacked by the etchant. Methylene chloride is an etchant of sulphur-based compounds, suggesting that the connecting phase is either PES or PES-rich. Fig. 9 also appears to show an unetched layer around 0.7 μm thick, surrounding the fibres, and careful observation of the central crack indicates that the crack path followed the particle/matrix interface. Figs 10 and 11 show T300/914 transverse tensile fracture surfaces obtained at − 40 °C and 140 °C, respectively. Plastic deformation of the connecting phase was greater at the higher temperature, providing further evidence that the connecting phase is thermoplastic and, therefore, PES-

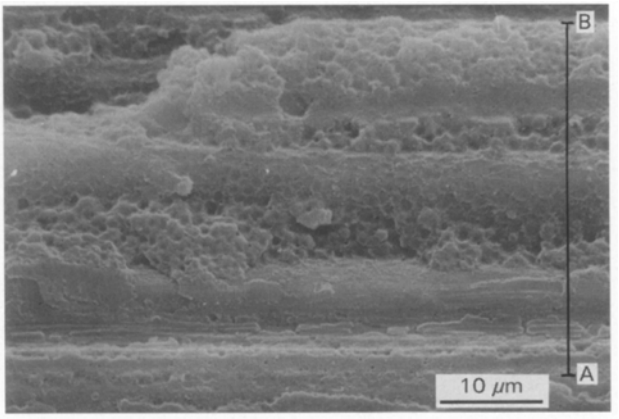

Figure 10 Unidirectional T300/914 transverse tensile fracture surface obtained at 10° mm min^{-1} and − 40 °C showing limited plastic deformation. The line AB corresponds to the section seen in Fig. 15.

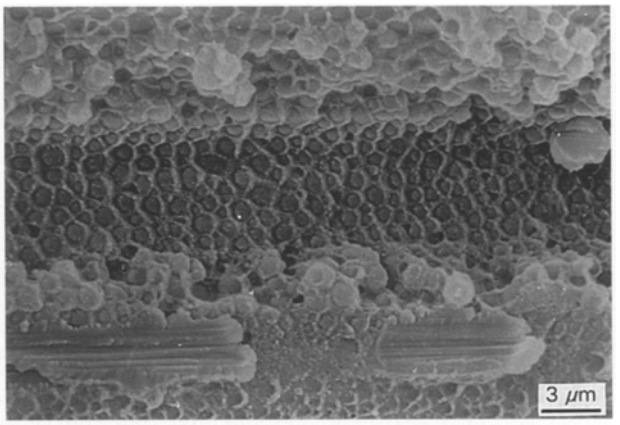

Figure 11 Unidirectional T300/914 transverse tensile fracture surface obtained at 10° mm min^{-1} and 140 °C showing extensive plastic deformation and regions of interphase material.

based. Several resin regions of ribbed surface morphology can be seen (e.g. at the bottom of Fig. 11). This ribbed pattern is known to exist on the fibre surface and so these regions must represent areas of fracture at the fibre/matrix interface and are fragments of the interphase region surrounding the fibres. On closer examination of selected etched composite surfaces where propagating cracks were observed, fracture at the fibre/matrix interface was only observed in areas of high fibre volume fraction, where the epoxy-based surrounding layer is mutually shared between two or more fibres. In other areas, fracture has occurred either wholly within the two-phase matrix, or at the interface between the two-phase matrix and the surrounding layer.

The horizontal centre third in Fig. 10 shows a fibre between two regions of resin structure. However, the surface of the fibre is not ribbed, but coated in a layer of resin on which a pattern of scars has developed. This scar pattern appears to represent the boundary between the surrounding layer (interphase) and the two-phase resin, as observed in Fig. 12 (obtained under standard conditions). The broken fibre on the right of Fig. 12 is noteworthy as the fracture surface morphology is planar, and not flexural as would be expected if fibre bridging has occurred. The scars are of crater-like appearance and can therefore be

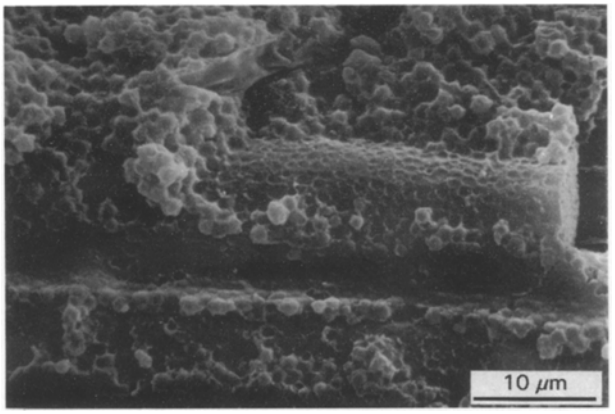

Figure 12 Unidirectional T300/914 transverse tensile fracture surface obtained at 10° mm min^{-1} and 23 °C revealing regions of "scar-like" structure bonded to the interphase region and the planar nature of the observed fibre fracture.

assumed to be the PES-based phase. Few, if any, epoxy particles are bonded to the interphase region, suggesting the presence of a relatively weak bond between these two phases.

4. Discussion

4.1. Structural modelling

4.1.1. Bulk resin

From Figs 8–12, the structure of the matrix appears identical in bulk form to that of a composite constituent, i.e. a two-phase structure consisting of a particulate phase (c. 0.8μm in diameter) embedded within a connecting matrix. Fig. 9 shows that this matrix is either PES or PES-based with the particulate phase being epoxy-based. This epoxy phase predominates in the resin, contributing over 85% of the total structure; therefore, the irregular areas of particulate phase observed in Fig. 9 are not surprising and represent areas where several particles have fused together. The only deformation observed within the two-phase resin occurs in the connecting matrix and increases with increasing temperature, again suggesting that this matrix is thermoplastic-based. As the volume fraction of the particulate phase is so high, the only realistic structural model for the resin is that of a three-dimensional hexagonal particulate array, as shown in Fig. 13a. This model, though, is highly simplistic as it does not account for the fused particulate regions observed in the fractographs.

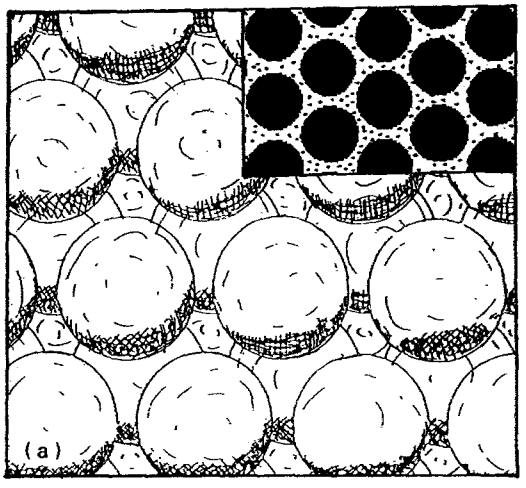

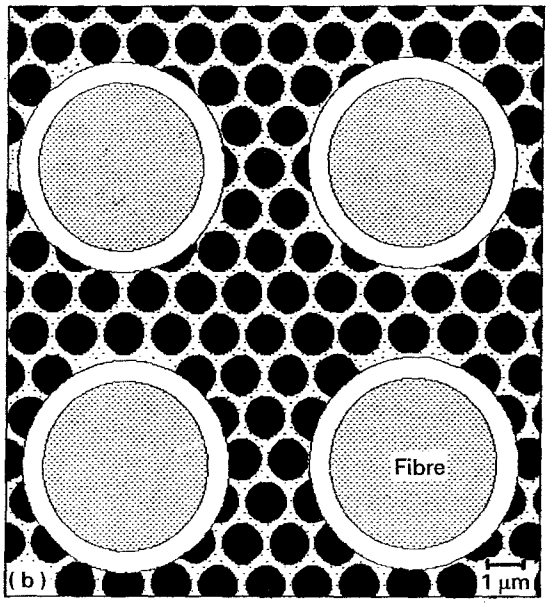

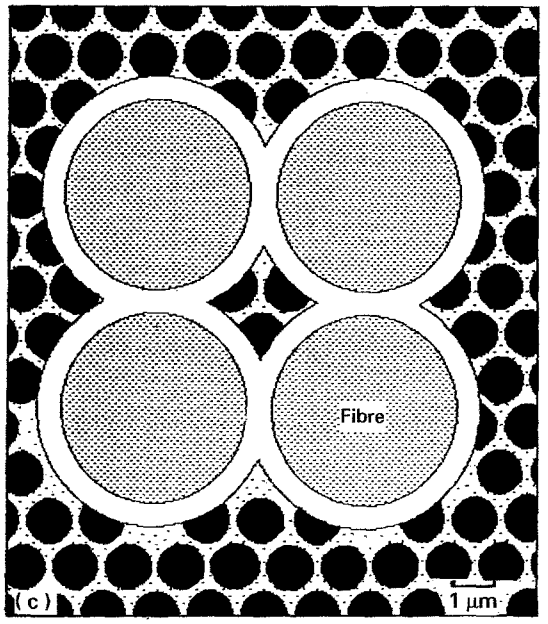

Figure 13 (a) Hexagonal particulate array representing the three-dimensional model developed for the two-phase resin. Inset: two-dimensional representation to be used in subsequent schematics. Particles are ca. 1 μm diameter. (b) Two-dimensional representation of unidirectional T300/914 in areas of low fibre volume fraction. (c) Two-dimensional representation of unidirectional T300/914 in areas of high fibre volume fraction showing interphase regions shared between fibres. White areas = interphase; light dotted areas = connecting phase; heavy dotted areas = fibres.

4.1.2. Composite

Fractographic observations have shown that the microstructure of the two-phase resin in the composite appears unchanged from that in the bulk resin material. However, there is a third resin phase present, manifesting itself in the form of a thin epoxy-rich uneven layer coating the fibres, that is mutually shared

by several fibres in areas of high fibre volume fraction, V_f. Fig. 13b shows the proposed two-dimensional structural model for unidirectional T300/914 in areas of low V_f and Fig. 13c represents the more complex model developed for the composite in areas of high V_f, and so T300/914 carbon fibre/epoxy composite is best modelled as a fibre-reinforced particle-filled thermoplastic. In keeping with previous modelling studies [26–28], a square array has been assumed.

4.2. Residual stress patterns

4.2.1. Bulk resin

With such a heterogeneous resin as 914, there will undoubtedly exist the problem of residual stresses. Over the temperature range examined, the macroscopic shrinkage stress varied between 38 (− 40 °C) and 4 MPa (140 °C). This stress is comparatively rather high [29]. In addition, the relaxed thermal stress was calculated and found to differ substantially from the macroscopic shrinkage stresses. This difference is probably due to microscopic stress patterns between the resin phases, and decreased with increasing temperature, supporting this argument.

The residual stress distribution of fibres embedded within a resin in a hexagonal array has been modelled in two dimensions by Chamis [30]. A modulus ratio ranging from 10–150 was used and the thermal shrinkage assumed corresponded to a typical fibre composite (not identified) with a cure differential of 300 °F. It was shown that the maximum tensile radial residual stress occurs at the six resin-rich symmetry axes, i.e. at $\theta = 30°, 90°, 150°, 210°, 270°$ and 330°, as shown in Fig. 14. It was also shown that the axial residual stresses at the fibre/matrix interface are tensile and at a maximum close to the particle boundary, and so it is probable that fracture in such a model would initiate in one or more of the shaded areas shown. Extension of this model into three dimensions results in a hexagonal particulate array. If the coefficients of thermal expansion of the two resin phases and the corresponding modulus values differ, then a structural model for the bulk 914 resin has also been approximated. Although the modulus ratio is likely to be smaller than in the Chamis model, such an approximation is reasonable, although the stress values exhibited will be lower than for the modulus range quoted. If a transverse tensile stress is applied to the model, fracture will preferentially occur at 90° or ± 30° to the applied load at the particle/matrix interface. This results in the characteristic two-phase resin fracture pattern seen in the fractographs.

Residual thermal stresses are expected to be present within the neat resin, but their magnitude and influence is unclear. The difference in coefficients of thermal expansion for homogeneous epoxy resin and neat polysulphone is large (approximately 40% [31]) and so should also be large between epoxy and PES (a similar system) resulting in the mechanical properties of 914 materials being influenced by residual stressing.

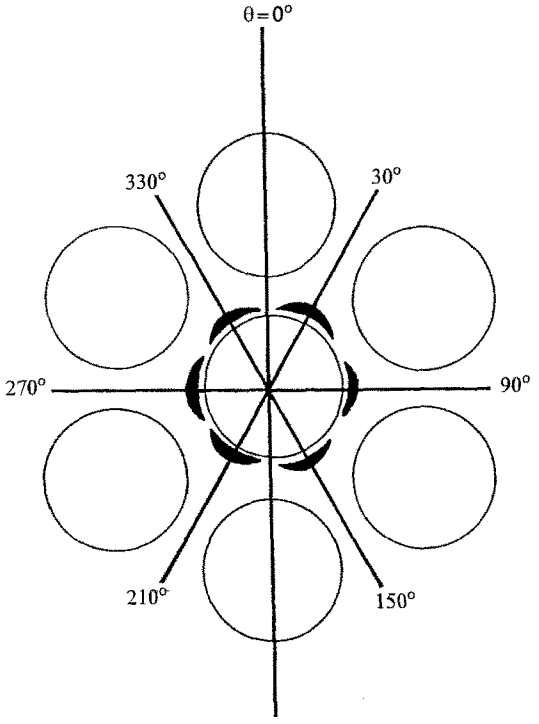

Figure 14 Showing the directions of maximum internal radial stress in a hexagonal array [30] and the regions of probable fracture initiation (shaded).

4.2.2. Composite

The stress distributions within the composite due to thermal and transverse mechanical loadings have been modelled by Allen [27]. For thermal stressing caused by cooling the material from the cure temperature to ambient temperature, the maximum principal tensile stress was shown to reach a peak of 36.1 MPa at close proximity to the interface. The addition of a transverse mechanical stress of 20 MPa was found to give a very similar, but slightly asymmetric, stress distribution. The peak stress of 49 MPa acted at an angle of 34° to the loading axis.

Allen's model is highly simplistic, and based on three assumptions. Firstly, a uniform square fibre array is assumed. Although the fibre distribution in the composite is irregular, sufficient areas will exist of approximately square array to justify this assumption. Secondly, a fibre volume fraction of 0.55 is assumed, which approximates to that for the material under test. Thirdly, the model assumes a homogeneous resin phase, which clearly does not apply to this system.

4.3. Application of the structural models to tensile fracture of the material

4.3.1. Toughening mechanisms

The thermoplastic-based component of the resin will almost certainly possess high toughness characteristics. For example, Nairn [32] quotes a fracture toughness of 1360 Jm^{-2} for neat polysulphone (a material of similar chemical and mechanical behaviour). The fracture toughness of bulk 914 resin is approximately 103 Jm^{-2} [33]. Therefore, the presence of the epoxy phase has reduced the toughness of the resin by behaving as rigid particles within a softer matrix material. It is well established [9, 34] that the toughness

of a polymer can be enhanced by the addition of a limited quantity of particulate phase. Low and Mai [35] have shown that increasing additions of zirconia to epoxy resin enhances the toughness in quantities up to 18% zirconia, whereupon it peaks and starts to decrease until a point is reached (ca. 40% zirconia) when the toughness of the reinforced resin becomes less than that of the bulk resin. In this brittle matrix/hard particle situation, the major toughening mechanisms include crack deflection and branching [9]. These are also contributory toughening mechanisms in the 914 resin. However, deformation of the connecting phase in this system is likely to become increasingly dominant as the temperature rises. In the 914 system, the amount of particulate phase present is very high (around 85%). It is likely that the toughness of the system would be improved by lowering the amount of particulate phase present, not only through a contribution from crack deflection mechanisms, but also through increased deformation potential in the connecting phase. This situation is also closely analogous to the increased upper shelf toughness seen in clean steels, where the volume fraction of manganese sulphide particles (hard particles) in steel (ductile matrix) has been reduced. In the 914 system, this may be achieved by changing the curing parameters or the initial chemical composition of the resin.

4.3.2. Stress/strain behaviour

The nature of the stress/strain curves indicated that on a microscale, there must be a small percentage of the material undergoing large plastic strains which on a macroscale translates to large amounts of plastic deformation but low fracture strains. The fractographic studies clearly show that the tensile fracture path in the two-phase resin follows the interface between the particles and connecting matrix. The Chamis model suggests that particle/matrix debonding occurs first, followed by fracture across the connecting matrix. As this matrix is of a thermoplastic nature, these small interparticle regions are able to deform through large plastic strains, thus explaining the stress/strain behaviour. The fractographic studies show that these plastic strains increase with increasing temperature and that as these areas are relatively very small, the total strain to failure on a macroscale is low.

4.3.3. Failure mechanisms

Fracture at the interphase/resin interface was by far the most common fracture mechanism observed in the composite. Occasionally, interphase/fibre debonding was observed, but only in areas of high fibre density. As no fracture within the interphase was observed in these areas, it can be assumed to be relatively strong. The morphology of the fractured fibre observed in Fig. 12 inferred that no fibre flexure has occurred prior to final fracture. This observation is consistent with there being no interfacial debonding, i.e. a strong fibre/matrix interface or a strong interphase region.

The fracture surface presented in Fig. 10 shows a typical matrix-dominated composite fracture surface, and this surface is schematically represented in Fig. 15. It identifies the fracture mechanisms previously discussed and shows the dominant nature of interphase/matrix interfacial failure.

The characteristic scar pattern seen typically in Fig. 12 is formed when the particulate phase is removed from the connecting phase, which remains bonded to the interphase. The depth of this scar pattern gives an indication of the amount of plastic deformation absorbed by the connecting phase. The circular scars are not of uniform size and as no pitting of the interphase is observed, the interphase must have formed and fully grown before large-scale growth of the particulate phase had initiated, i.e. the particles will have grown on to the interphase rather than into it. It would therefore seem likely that the bond between the particulate phase and the interphase is weak, and will dominate the fracture process. The proposed mechanism behind fracture at the interphase/resin interface is schematically shown in Fig. 16. Under an applied load, the particulate phase debonds from the interphase (a) followed by cracking at the particle/connecting phase boundary as predicted by

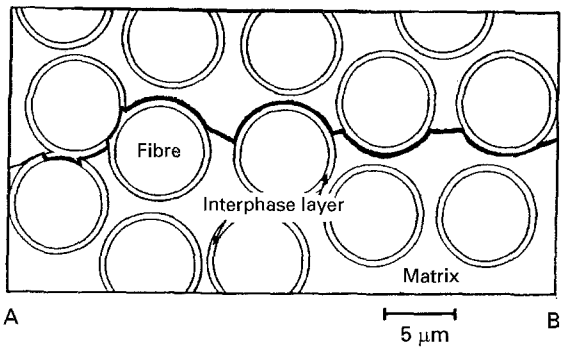

Figure 15 Schematic representation of the transverse tensile fracture path observed in Fig. 10 (side view). The thick line represents the fracture surface seen in Fig. 10.

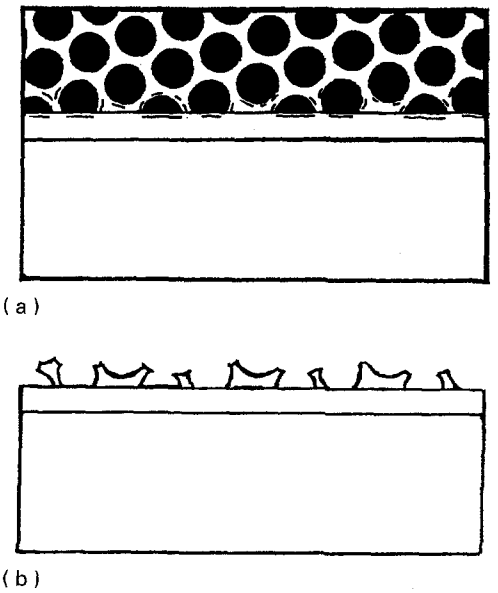

Figure 16 Schematic representation of failure in the composite at the interphase region. Microcracks form at the particle/matrix interface and separation of the particles from the interphase occurs (a). Rupture of the connecting matrix (b) results in a pattern of resin scars bonded to the interphase. White areas = interphase; light dotted areas = connecting phase; heavy dotted areas = fibres.

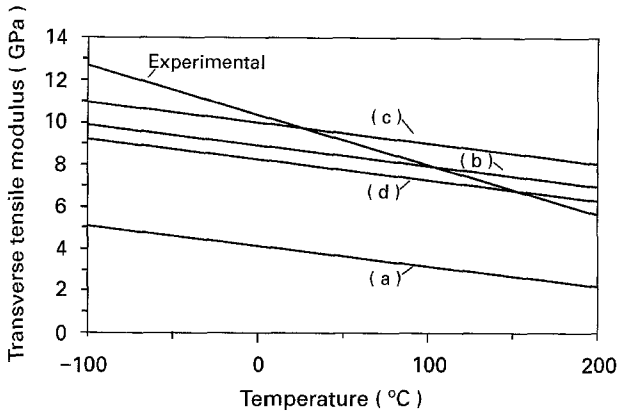

Figure 17 Variation of transverse tensile modulus with temperature using experimental data and modulus predictions from constituent properties from (a) rule of mixtures, (b) modified rule of mixtures, (c) Chamis model, and (d) Spencer model.

the Chamis model. Final fracture occurs (b) when these cracks propagate through the connecting phase.

4.4. Tensile property modelling

4.4.1. Modulus prediction

Prediction of the transverse modulus behaviour over the temperature range from constituent mechanical properties has been attempted using some of the more widely known models in current use, and Fig. 17 details in graphical form the values of $E_{\perp T}$ obtained from these models, compared to the experimentally determined modulus values. The predictive models selected are as follows.

(a) The simple rule of mixtures [36]

$$E_{\perp T} = \frac{E_f E_r}{E_f(1 - V_f) + E_r V_f} \tag{7}$$

where E_f is the fibre modulus (taken as 13.8 GPa [23] and assumed to be independent of temperature) and E_r is the resin tensile modulus and V_f is the fibre volume fraction.

(b) The modified rule of mixtures [36], accounting for Poisson contraction of the resin

$$E_{\perp T} = \frac{E_f E_{r*}}{E_f(1 - V_f) + E_{r*} V_f} \tag{8}$$

where

$$E_{r*} = \frac{E_r}{1 - \nu_r^2} \tag{9}$$

(ν_r being the matrix Poisson's ratio).

(c) The Chamis model [37], that utilizes the anisotropy of the composite

$$E_{\perp T} = \frac{E_r}{\left[1 - (V_f)^{1/2}\left(1 - \frac{E_r}{E_f}\right)\right]} \tag{10}$$

(d) The Spencer model [38], that accounts for the strain distribution throughout the composite by the use of a fibre separation parameter, (γ)

$$\frac{E_{\perp T}}{E_r} = \frac{\gamma - 1}{\gamma} + \frac{1}{X}\left[-\frac{\pi}{2} + \frac{2\gamma}{(\gamma^2 - X^2)^{1/2}} \times \tan^{-1}\left(\frac{\gamma + X}{\gamma - X}\right)^{1/2}\right] \tag{11}$$

where

$$X = 1 - \frac{E_r}{E_f} \tag{12}$$

and γ is defined as

$$\gamma = \frac{1}{(1.8V_f - 0.75V_f^2)^{1/2}} \tag{13}$$

For the composite in this study, V_f was measured as 0.57 (using a resin burn-off technique). Numerous other property models exist, but the four chosen appear to be the most frequently used.

Fig. 17 has been constructed using constituent modulus data from several different temperatures and clearly shows that another factor must be considered to obtain accurate property modelling over the temperature range. This factor can only be the interphase region and so terms such as E_i (interphase modulus) and V_i (interphase volume fraction) need to be added to the predictive modelling process. The Chamis model appeared to yield the best modulus prediction at standard temperature, although the absence of interphase terms renders it inapplicable at all other temperatures.

4.4.2. Modelling of the interphase

The predictive models mentioned previously do not account for the interphase component. However, accurate modulus prediction over the temperature range should be possible if the interphase properties are known. Conversely, it should be possible to predict the interphase properties providing the relevant composite and constituent properties are known. For example, consider the basic Halpin–Tsai relationship [38]

$$\frac{E_{\perp T}}{E_T} = \frac{(1 + \zeta\eta V_f)}{(1 - \eta V_f)} \tag{14}$$

where

$$\eta = \left(\frac{E_f}{E_r} - 1\right)\Big/\left(\frac{E_f}{E_r} + \zeta\right) \tag{15}$$

and ζ is a fibre arrangement factor ($\zeta = 2$ for square arrays and $\zeta = 1$ for hexagonal arrays). A reasonable estimation for ζ has been obtained by Hewitt and Malherbe [39] in terms of fibre volume fraction and for a V_f of 0.57, $\zeta = 1.145$. This relationship results in an inaccurate prediction of $E_{\perp T}$ at all temperatures as no interphase terms are present.

Equation 16 presents a modified Halpin–Tsai model, which now takes into consideration E_i and V_i, the interphase modulus and volume fraction, respectively

$$\frac{E_{\perp T}}{E_{r*}} = \frac{1 + \zeta\eta(V_f + V_i)}{1 - \eta(V_f + V_i)} \tag{16}$$

where

$$\eta = \left(\frac{E^*}{E_{r*}} - 1\right)\Big/\left(\frac{E^*}{E_{r*}} + \zeta\right) \tag{17}$$

and

$$E^* = \frac{E_f E_i}{1.15(E_f V_i + E_i V_f)} \tag{18}$$

Equation 16 accounts for the Poisson behaviour of the resin and it assumes a fibre diameter of 7 μm and an interphase of 1 μm uniform thickness (taken from Fig. 9). It also assumes that the interphase region is shared by more than one fibre, because the resulting volume fraction ($V_f + V_i$) of 0.87 is too large to be modelled as a square or hexagonal array (i.e. modelled according to Fig. 13c).

This model was found to function at all temperatures within the temperature range and gave values for the interphase modulus that were between $E_{\perp T}$ and E_r i.e. the interphase is stiffer than the two-phase matrix. This is not surprising, because the interphase has been shown to be epoxy based, whereas the two-phase matrix possesses a softer thermoplastic component. Also, Fig. 3 shows that the modulus behaviour of the composite is different to that of the neat resin, i.e. dE/dT is different for the two materials. This is explained by the above model, because if E_i was calculated using constituent data from other temperatures, it possessed a dE/dT value different to that for the neat resin, as shown in Fig. 18.

4.4.3. Strength prediction

The interphase has no discernible influence on the strength of the composite. The $d\sigma/dT$ values for the composite and the bulk resin appear identical (Fig. 1), and so development of strength models that account for the interphase are unnecessary. Prediction of strength is difficult, as micromechanical phenomena such as inherent flaws, are usually difficult to consider. Also, most property models regard the fibres as weaknesses, whereas in T300/914, the fibres act as strengtheners. However, the Tsai-Hahn strength equation as used by Ha and Springer [40] relates strength to K_T, the transverse tensile stress concentration factor, and Σ, the stress partitioning factor, and therefore have the capacity to model accurately the strength of the material by an arbitrary definition of these factors using curve fitting, i.e.

$$\sigma_\perp = \frac{1 + V_f\left(\frac{1}{\Sigma} - 1\right)\sigma_r}{K_T} \quad (19)$$

where σ_r is the resin strength and $\sigma_\perp$ the composite strength. Σ takes a value of 0.928 whilst K_T takes a value of 0.044. Any further strength modelling will require improved resin strength data which are not yet available.

4.5. A probable cure mechanism for the composite

The results presented in this study provide a strong case for there being a multistage curing mechanism whereby the two epoxy-based phases form at different times, resulting in the formation of the weakest regions in the composite: the particle/interphase boundary. Fig. 19 schematically details the curing mechanism that is thought to exist in the formation of T300/914 based on the information collated from this study. Initially, the resin exists as a homogeneous matrix (a). At the start of the cure cycle, two co-

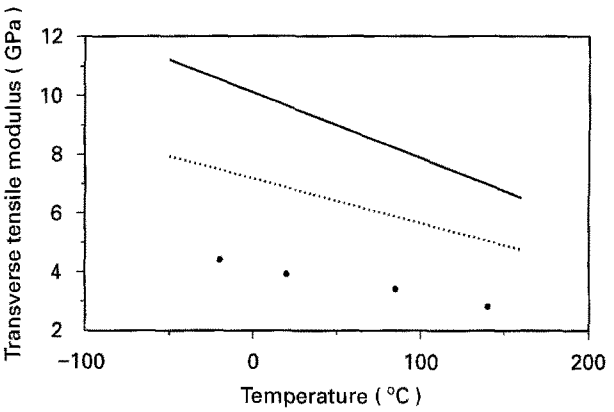

Figure 18 Variation of (—) composite tensile modulus, (●) resin tensile modulus [25] and (···) interphase tensile modulus (Equation 16) with temperature.

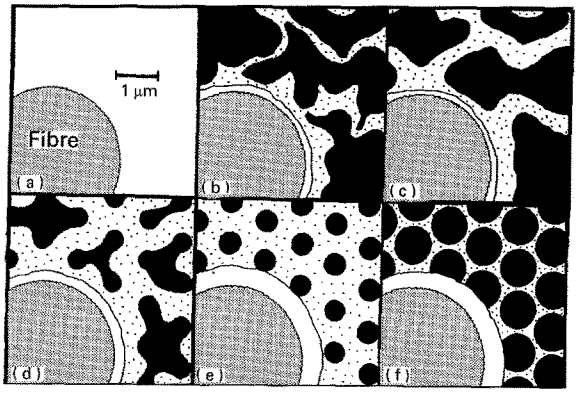

Figure 19 Schematic illustration of stages in the probable curing mechanism for T300/914. (a) Initial homogeneous resin blend. (b) Phase separation and formation of interphase region. (c, d) Growth of interphase and further phase separation. (e) Particulation of epoxy phase and cessation of interphase growth. (f) Completion of cure. White areas = interphase; light dotted areas = connecting phase; heavy dotted areas = fibres.

connective phases form and an epoxy-based interphase layer forms on the fibre surface (b). On further curing, the phase connectivity is interrupted by an increase in interfacial tension leading to the particulation of the epoxy-based phase. These particles then grow by removal of epoxy-based material from the connecting phase according to the cure parameters, and these particles will occasionally grow into one another, forming large clusters. It would appear that the fibres act as nucleation sites for the epoxy phase, i.e. "ready made particles" resulting in early formation and growth of epoxy-based layers around each fibre that occasionally merge into one another in areas of high V_f. These layers continue to grow to their full size whilst the two-phase co-continuous structure starts to separate (d). Eventually, interphase growth is arrested, one matrix phase particulates (e) and then grows in preference to the interphase until the maximum particle diameter is realized (f). Particles that nucleated at a distance from the interphase less than the eventual maximum particle diameter have their growth suppressed, once contact with the interphase is achieved, resulting in truncated spheres. As the two phases do not grow into one another, only a very weak bond will exist between them and the truncated particles around the interphase result in a scar pattern of various crater diameters on fracture.

5. Conclusion

914 resin is a two-phase resin consisting of epoxy-based particles approximately 1 μm in diameter, embedded within a thermoplastic PES-based connecting phase and therefore this system behaves as a particle-reinforced thermoplastic. Fracture within the resin preferentially occurs at the particle/matrix interface. An additional phase exists within the composite in the form of an epoxy-based interphase around 0.7 μm thick, surrounding the fibres. The interphase/fibre interface is relatively very strong and failure in this region is only observed in areas of high V_f where the interphase is mutually shared between fibres. The weakest point in the composite is the interphase/particle interface and fracture preferentially occurs in these regions.

Although highly simplistic, the structural models developed for the resin and composite provide the basis for accurate mechanical property prediction once mechanical data have been obtained for the individual resin phases. The interphase and the particulate phase appear to have been formed at different times in the cure cycle. It may also be that they are of different chemical composition, although this has yet to be determined.

The observations reported in this study provide basic insights into a rather complex structure of a commonly used composite system. The toughening mechanisms at work within the material have been explained using the structural models and clearly the addition of PES has increased the toughness of the base epoxy resin, but it has also caused the formation of a complex internal stress field which has weakened the material. From the evidence obtained, a realistic curing mechanism has been developed and it is obvious that for a system such as T300/914, a fuller understanding is required into the effect of altering the composition and curing of the material before the maximum potential in terms of mechanical behaviour can be realized.

The stress/strain behaviour of unidirectional T300/914 under transverse tensile loading has been explained using the structural models developed. The structural models have also been used successfully to predict the fracture mechanisms under this type of loading.

The viscoelastic response of the composite on a macroscale (modulus) is different to that on a microscale (strength and fracture strain). Also, the interphase region has an influence over the temperature range -40 to 140 °C on a macroscale but not on a microscale, suggesting that this interphase region does not play a role in the fracture of the material, but does contribute to the overall stiffness of the material.

Acknowledgements

The author thanks Professor Derek Hull for the use of the facilities at the Department of Materials Science, University of Cambridge, and also all the staff and colleagues who helped in this work both in Cambridge and overseas.

References

1. J. A. LEE and D. L. MYKKANEN, "Metal and Polymer Matrix Composites" (Noyes Data Corporation, Park Ridge, N.J., 1987).
2. Ciba-Geigy Information Sheet FTA49e (1984).
3. A. J. BARKER and V. BALASUNDARAM, *Composites* **18** (1987) 217.
4. "D3039-76 ASTM Annual Book of Standards" (American Society for Testing and Materials, Philadelphia, PA, 1985).
5. P. T. CURTIS, RAE Technical Report (1985).
6. P. D. EWINS, RAE Technical Report TR71217 (1971).
7. R. A. ELKIN, G. FUST and D. P. HANDLEY, "Composite Materials: Testing and Design," ASTM STP460 (American Society for Testing and Materials, Philadelphia, PA, 1969) pp. 321–335.
8. G. H. GOODMAN, "Handbook of Thermoset Plastics" (Noyes, Park Ridge, N.J., 1986).
9. A. C. GARG and Y.-W. MAI, *Compos. Sci. Technol.* **31** (1988) 179.
10. F. J. MCGARRY, *Proc. R. Soc. Lond.* **A319** (1970) 59.
11. C. B. BUCKNALL, "Toughened Plastics" (Applied Science, London, 1977).
12. S. K. DOUGLASS, P. W. R. BEAUMONT and M. F. ASHBY, *J. Mater. Sci.* **15** (1980) 1109.
13. W. D. BASCOM, R. L. COTTINGTON, R. L. JONES and P. PEYSER, *J. Appl. Polym. Sci.* **19** (1975) 2545.
14. A. C. MALONEY, H. H. KAUSCH and H. R. STEIGER, *J. Mater. Sci.* **18** (1983) 208.
15. A. J. KINLOCH, D. MAXWELL and R. J. YOUNG, *ibid.* **20** (1985) 4169.
16. K. YAMANAKA and T. INOUE, *Polymer* **30** (1989) 662.
17. C. B. BUCKNALL and I. K. PARTRIDGE, *Polymer* **24** (1983) 639.
18. *Idem, Br. Poly. J.* **15** (1983) 71.
19. P. A. SMALL, *J. Appl. Chem.* **3** (1953) 71.
20. J. W. CAHN, *J. Chem. Phys.* **42** (1965) 93.
21. I. GURNELL, Ciba-Geigy, Duxford (1991) private communication.
22. Rolls Royce Process Specification MSRR9270 (1990).
23. Ciba-Geigy Information Sheet FTA49e, August (1984).
24. J. W. JOHNSON, *Phil. Trans. R. Soc. Lond.* **A294** (1980) 487.
25. M. FISCHER, Purchase Order EP3114842P Report 1, Ciba-Geigy, Marly (1989).
26. C. B. ALLEN, "Parametric Analysis on the Micromechanics Modelling of Composite Materials", Report SMR00023 Rolls Royce plc, August 1988.
27. C. B. ALLEN, private communication (1989).
28. *Idem*, Rolls Royce Report MEGO34324, October 1990.
29. Z. QUSEN and L. YUHUA, in "ICCM VII: Seventh International Conference on Composite Materials", edited by W. Yunshu, N. C. R. Buskell, J. M. Hodgekinson and J. Morton, Vol. 1 (Pergamon Press, Guangzou, 1989) p. 386.
30. C. C. CHAMIS, in "Composite Materials", Vol. 6, edited by E. P. Plueddemann (Academic Press, New York, 1974) p. 31.
31. J. A. NAIRN and P. ZOLLER, *J. Mater. Sci.* **20** (1985) 355.
32. J. A. NAIRN, *J. Comp. Mater.* **21** (1987) 798.
33. A. J. BARKER and V. BALASUNDARAM, *Composites* **18** (1987) 217.
34. P. W. R. BEAUMONT, in "Fracture Mechanics: Current Status, Future Prospects" edited by R. A. Smith (Pergamon, Cambridge, 1979).
35. I. M. LOW and Y.-W. MAI, *Compos. Sci. Technol.* **33** (1988) 191.
36. D. HULL, "Introduction to Composite Materials" (Cambridge University Press, 1981).
37. C. C. CHAMIS, *SAMPE Q.* April (1984) 14.
38. J. C. HALPIN, *J. Compos. Mater.* **3** (1969) 732.
39. R. L. HEWITT and M. C. de MALHERBE, *ibid.* **4** (1970) 280.
40. S. K. HA and G. C. SPRINGER, in "ICCM VI: Sixth International Conference on Composite Materials and ECCM 2: Second European Conference on Composite Materials", edited by F. L. Matthews, N. C. R. Buskell, J. M. Hodgekinson and J. Morton. Vol. 4 (Elsevier, London, 1987) pp. 422–8.

Received 23 August 1994
and accepted 15 August 1995